McCune-Albright Syndrome: A Detailed Pathological and Genetic Analysis of Disease Effects in an Adult Patient

Vladimir Vasilev,* Adrian F. Daly,* Albert Thiry,* Patrick Petrossians, Frederic Fina, Liliya Rostomyan, Monique Silvy, Alain Enjalbert, Anne Barlier, and Albert Beckers

Departments of Endocrinology (V.V., A.F.D., P.P., L.R., A.Be.) and Pathological Anatomy (A.T.), Centre Hospitalier Universitaire de Liège, University of Liège, Domaine Universitaire du Sart Tilman, 4000 Liège, Belgium; Department of Biological Oncology Transfer (F.F.), Laboratory of Medical Biology, Assistance Publique-Hôpitaux de Marseille, 13354 Marseille, France; and Laboratory of Biochemistry and Molecular Biology (M.S., A.E., A.Ba.), Centre Hospitalier Universitaire Conception, University of the Mediterranean, 13007 Marseille, France

Context: McCune Albright syndrome (MAS) is a clinical association of endocrine and nonendocrine anomalies caused by postzygotic mutation of the *GNAS1* gene, leading to somatic activation of the stimulatory α-subunit of G protein (Gsα). Important advances have been made recently in describing pathological characteristics of many MAS-affected tissues, particularly pituitary, testicular, and adrenal disease. Other rarer disease related features are emerging.

Objective: The objective of the investigation was to study the pathological and genetic findings of MAS on a tissue-by-tissue basis in classically and nonclassically affected tissues.

Design: This was a comprehensive autopsy and genetic analysis.

Setting: The study was conducted at a tertiary referral university hospital.

Patients: An adult male patient with MAS and severe disease burden including gigantism was the subject of the study.

Intervention(s): Interventions included clinical, hormonal, and radiographic studies and gross and microscopic pathology analyses, conventional PCR, and droplet digital PCR analyses of affected and nonaffected tissues.

Main Outcome Measure: Pathological findings and the presence of *GNAS1* mutations were measured.

Results: The patient was diagnosed with MAS syndrome at 6 years of age based on the association of café-au-lait spots and radiological signs of polyostotic fibrous dysplasia. Gigantism developed and hyperprolactinemia, hypogonadotropic hypogonadism, and hyperparathyroidism were diagnosed throughout the adult period. The patient died at the age of 39 years from a pulmonary embolism. A detailed study revealed mosaiscism for the p.R201C *GNAS1* mutation distributed across many endocrine and nonendocrine tissues. These genetically implicated tissues included rare or previously undescribed disease associations including primary hyperparathyroidism and hyperplasia of the thymus and endocrine pancreas.

Conclusions: This comprehensive pathological study of a single patient highlights the complex clinical profile of MAS and illustrates important advances in understanding the characteristics of somatic *GNAS1*-related pathology across a wide range of affected organs. **(*J Clin Endocrinol Metab* 99: E2029–E2038, 2014)**

ISSN Print 0021-972X ISSN Online 1945-7197
Printed in U.S.A.

Received January 31, 2014. Accepted July 11, 2014.
First Published Online July 25, 2014

* V.V., A.F.D., and A.T. contributed equally to this work.

Abbreviations: FD, fibrous dysplasia; MAS, McCune Albright syndrome; MRI, magnetic resonance imaging.

McCune Albright syndrome (MAS) is a very rare sporadic genetic disorder that comprises a triad of polyostotic fibrous dysplasia (FD), café-au-lait skin pigmentation, and precocious puberty (1, 2). MAS can affect a wide range of tissues beyond the classical triad, including endocrine organs (pituitary, thyroid, and adrenals), the gastrointestinal tract, and others (3, 4). MAS is caused by somatic missense mutations of the *GNAS1* gene, which lead to constitutional activation of Gsα protein, raised cAMP, and increased cellular activity and growth (5–7). In MAS the *GNAS1* mutation is believed to occur postzygotically, leading to mosaiscism for mutation-bearing cells and hence a variable pattern in the variety and extent of affected tissues. The burden of disease in MAS varies significantly, and partial or incomplete forms of MAS have been described (8). Craniofacial FD, in particular, can vary widely in severity from asymptomatic to severe disfigurement and functional impairment. Craniofacial FD may be severe in MAS patients with pituitary somatotrope hyperfunction causing GH excess (9). Given the rarity of MAS and the lack of an animal disease model, the clinical epidemiology of MAS is only now being comprehensively elucidated in long-term collaborative efforts that have defined important features like gonadal pathology in males and the management of MAS-related pituitary disease (9, 10).

Few comprehensive anatomopathological studies have been published in subjects with MAS. We describe a patient with MAS with a heavy disease burden comprising deforming craniofacial and axial skeletal FD and gigantism that contributed to his early death. A comprehensive pathological and genetic study at postmortem provided a unique insight into the pathology and genetics of a variety of MAS-related abnormalities, both classical and rarely described/novel, underlining the multiple major and minor disease manifestations in MAS.

Materials and Methods

Case history

A 35-year-old male was referred to our clinic for evaluation and monitoring. He had been diagnosed with MAS at 6 years of age based on the presence of café-au-lait macules (lower back and right arm) and radiological signs of polyostotic FD in addition to precocious puberty. At original presentation he was well above the 97th centile for height (135 cm) and weight (29 kg) (Figure 1). He had associated facial asymmetry due to marked right-sided skull base expansion. Extensive upper and lower limb bony involvement was present. The cranial nerve examination revealed a mild loss of visual acuity in the right eye and an impingement on the upper nasal field of the left eye. There was hearing loss on the right ear. The skeletal pathology progressed rapidly through childhood and adolescence, becoming particularly severe in the vertebrae, hips (right sided osteosynthesis required), and cranial bones. These latter changes led to the displacement of the left eye laterally and development of marked asymmetry of the face and jaw. The hip pathology progressed, with a right-sided coxa vara developing, and at the age of 13 years, a right-sided osteosynthesis of the hip was performed.

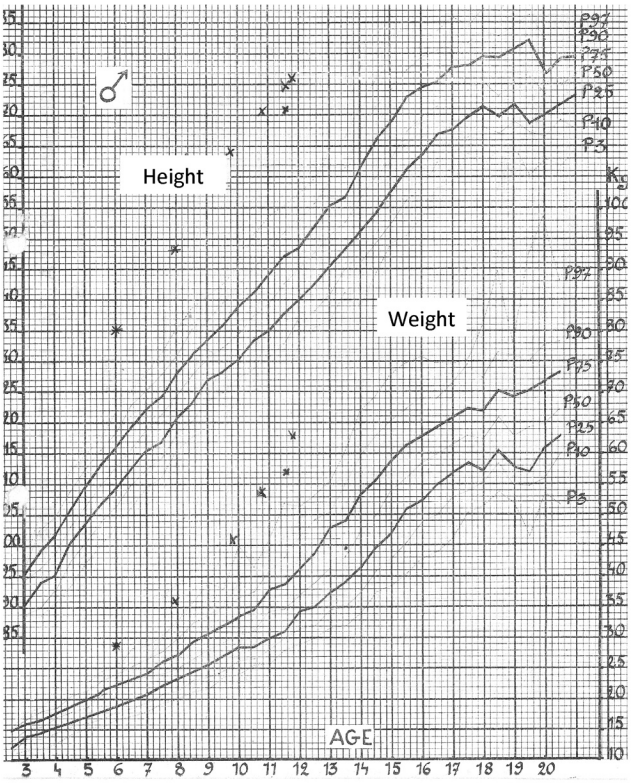

Figure 1. The patient's original pediatric growth chart shows height and weight above the 97th centile at presentation, when aged 6 years. His gigantism progressed throughout childhood in parallel with the development of marked craniofacial FD and hip disfigurement, and at the age of 12 years, his height was already 176 cm.

Aged 11 years, the patient's pubertal development was P3, G3, A1; gonadal, thyroid and adrenal hormone profiles were normal. The patient's height increased and he reached 186 cm by the age of 13 years. Imaging of the sella revealed no enlargement or evidence of a pituitary tumor. Basal GH levels were consistently elevated (10–20 ng/mL; normal < 3 ng/mL), with a paradoxical increase after an oral glucose load. He also had moderate hyperprolactinemia at about 2.5 times the upper limit of normal. Treatment with bromocriptine had no noticeable effect on GH levels (somatostatin analogs were unavailable at that time and neurosurgery was declined). Radiological changes in the distal phalanges were typical of the deformation seen in acromegaly. The subsequent evolution was marked by progressive vertical growth reaching a final adult height of 205 cm, further coarsening of facial features, acral growth, multiple bone deformities, and worsening craniofacial FD (Figure 2), with pathological fractures within the FD affected regions (right and left femoral neck, left femoral shaft, and left elbow), with bilateral hip prostheses required and scoliosis that required surgery. Biochemically and hormonally the patient exhibited persistent GH excess with concomitant hyperprolactinemia, which was treated with a long-acting somatostatin analog, although GH and IGF-1 remained elevated.

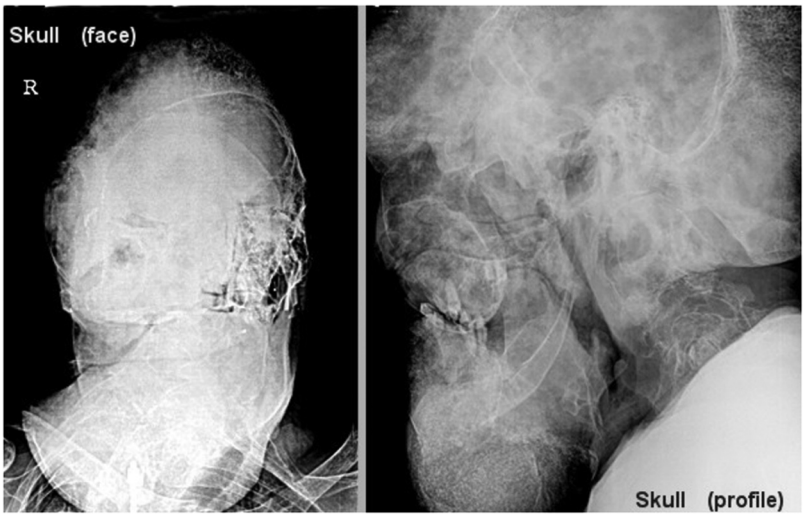

Figure 2. Radiological images demonstrating severe craniofacial FD in a MAS patient with gigantism. Plain skull radiographs of the patient at the age of 30 years show massive bone overgrowth affecting the entire skull, particularly the occipital bones, in addition to deforming enlargement of the mandible.

By the age of 30 years, the patient had developed hypogonadotropic hypogonadism (LH and FSH below the limit of quantitation, T 2.7 nM). Subsequently, primary hyperparathyroidism was diagnosed [total calcium: 10.6 mg/dL (upper limit of normal: 10.4 mg/dL); PTH: 104 pg/mL], which was associated with symptomatic nephrolithiasis of the right kidney. Thyroid and adrenal function measures were normal. By that time, brain magnetic resonance imaging (MRI) showed a normally proportioned pituitary gland that was accompanied by a large inferior sellar cystic lesion. There was profound facial, cranial, and cervical vertebral deformity, with the FD causing marked displacement of the cerebral parenchyma as illustrated in Figure 3 (see also video in Supplemental Figure 1, A and B). He was completely blind in the left eye. Addition of cabergoline to that of lanreotide Autogel successfully controlled IGF-1 (but not GH) and hyperprolactinemia. The patient presented to the emergency room with a severe iron-deficiency anemia of a suspected gastrointestinal source; endoscopy showed a Barrett's esophagus and polyps in the pylorus of the stomach (although no active bleeding source). Megacolon was also diagnosed.

The patient remained stable for 4 years after presentation to our department. At the age of 39 years, he collapsed and fell at home, which was associated with medullary compression and quadriplegia, and he died due to a cardiorespiratory arrest. On autopsy, a pulmonary embolism with lung infarction was determined as the primary cause of death. Particular attention was paid to investigating the role of MAS at a tissue and organ level to fully capture the disease burden.

Light microscopy and immunohistochemistry

Tissue fragments obtained from organs were fixed in 10% buffered formalin and embedded in paraffin; 5-μm-thin sections were then cut and stained with hematoxylin and eosin, periodic acid-Schiff reaction, and Foot's stain for light microscopy. An immunohistochemical analysis was performed on deparaffinized and dehydrated 5-μm tissue sections using the Dako EnVision system and the peroxidase/diethylaminobenzidene detection kit (Dako), according to the manufacturer's instructions. Immunostaining for chromogranin A, synatophysin, and inhibin was performed using monoclonal antibodies (Dako) diluted 1:600, 1:2, and 1:150, respectively; for CD56 staining the monoclonal antibody from Novocastra was used after 1:150 dilution. Positive control sections were prepared from lung carcinoid tumor and normal testis for inhibin. Negative controls were obtained by replacing the primary antibody with Tris-buffered saline.

Genetic studies

DNA was obtained from formalin-fixed tissues and paraffin-embedded fragments after digestion with proteinase K using commercially available kits (QIAGEN) as previously described (11). After purification of proteolysis residues, the final samples of DNA were washed with 70% ethanol and quantified with an UV spectrophotometer. Prior to PCR amplification, DNA samples were incubated for 1 hour at 37°C in the presence of BSA (12).

Mutation detection was performed by standard PCR amplification followed by sequencing of the *GNAS1* gene. Selective enrichment of the mutant allele was achieved by specific endonuclease digestion of the PCR product from the normal gene, as described previously (13, 14). Each test included a control sample that consisted of DNA heterozygous for the p.R201C mutation that was diluted 1:10 with wild-type DNA. It was detected as wild type after a single round of PCR but as heterozygous after the en-

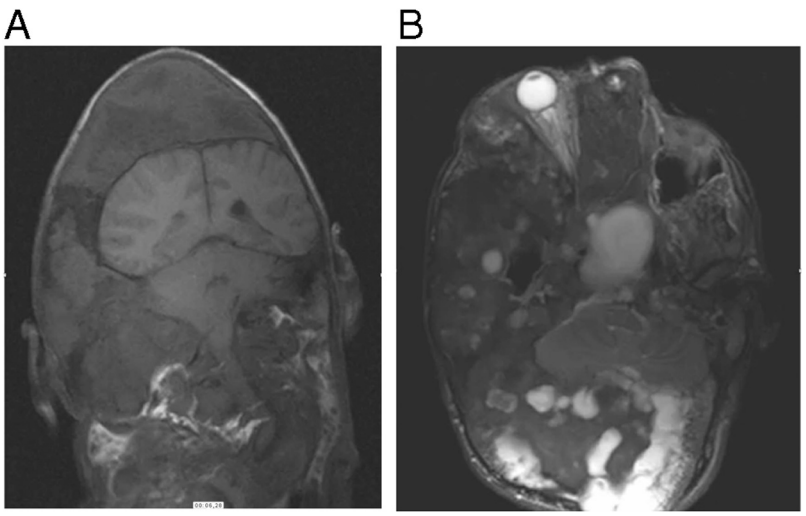

Figure 3. Coronal (A) and axial (B) MRI features in the MAS patient demonstrating profound craniofacial FD and related impingement of the brain and displacement of the optic nerves and eyes.

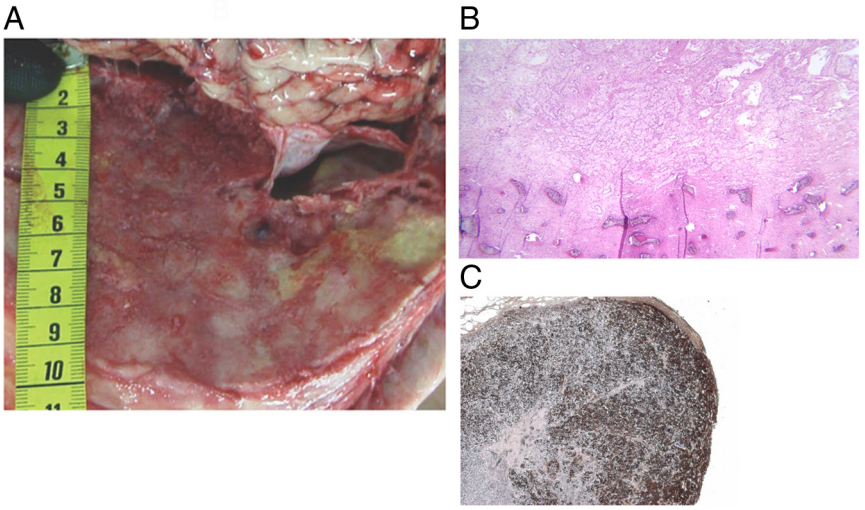

Figure 4. Pathological findings in tissues studied postmortem. Panel A illustrates the marked thickening of the skull due to craniofacial FD, while Panel B shows light microscopy of an affected region of bone pathology. Panel C shows pituitary gland with positive immunostaining for GH (brown) of an adenoma against a background of diffuse somatotrope hyperplasia.

richment procedure. This led us conclude that the mutant allele is present in at least 10% of the cells from tissues found to be heterozygous after enrichment. Using numerical PCR (15) in droplets (16) (ddPCR; Bio-Rad Laboratories), we measured the proportion of *GNAS1* p.R201C mutation in DNA samples. Five microliters of DNA were used in the presence of ddPCR supermix for Probes (Bio-Rad Laboratories). With ddPCR, the sample is dispensed so that each DNA molecule is localized in a distinct reaction chamber. In contrast to conventional PCR, ddPCR scatters the reaction in a large number of partitions studied individually. Sample partitioning allows the counting of molecules according a Poisson's distribution. Consequently, each reaction chamber contains either zero or one molecule, namely a negative or a positive reaction, respectively. After PCR amplification, nucleic acids can be quantified by counting the positive reactions. The number of positive tests related to the total number of analyses performed provides an absolute quantification. ddPCR permits the reading of 15 000–16 000 droplets per sample. Primers and hydrolysis probes sequences together with ddPCR conditions are available on request.

Results

At autopsy there were typical features of acrogigantism, and the patient measured 200 cm in length. Extensive vertebral scoliosis, external flexion of the right leg, and significant lower limb muscle atrophy were also observed. Thickening of the frontal bone and a large mandibular tumor contributed to the skull deformity. Café-au-lait lesions were present in the right lower thoracic region and on the right arm.

Skeletal system

The pathological findings in the skeleton consisted of cortical hyperplasia, cysts secondary to bone destruction in the medulla and lesions of fibrous dysplasia presenting either as diffuse hyperplasia or bone tumors. Long bones exhibited increased cortical thickness, but the density was decreased in areas with multiple medullar cysts containing fibrous tissue. The right humerus, femur, and most of the right side of the skull displayed pseudotumoral features with severe and diffuse expansion of the medulla. Light microscopy revealed sclerotic areas, areas of proliferation with a fibrodysplasic appearance, and necrotic fields with hemorrhage.

Craniofacial fibrous dysplasia

The full extent of the skull abnormalities in this patient are illustrated in Figure 2, with simple radiographs demonstrating the mandibular distortion due to a bone tumor. The craniofacial FD led to marked compression of the brain and spinal cord, with these elements echoing the previously established radiological findings (Figure 3). These changes are shown in situ in Figure 4A. A large, well-delineated tumor was found on the right side of the mandible. It had a heterogeneous histological structure with fibrous and dense bone tissue predominating in the central area, whereas the periphery displayed regions of neovascularization and metaplastic bone formation (Figure 4B).

Central nervous system

Both cerebral hemispheres presented flattening and deformities of the frontoorbital region due to bone compression (Figure 3). Except for diffuse cerebral edema, there were no macroscopic or microscopic brain or spinal cord lesions.

Skin

The epidermal structure and thickness were normal. The superficial and deep dermis was hyperplastic with a concentric and lamellar distribution of collagen bundles around skin appendages. Collagen bundles appeared broad and densely packed using Masson's trichrome stain and orcein staining showed dystrophic elastic fibers with irregular size and focal fragmentation. On immunohistochemistry, factor XIIIa positive dermal dendrocytes type 1 were scattered, globular, and of small size.

Endocrine system

Pituitary

The pituitary was enlarged and occupied an enlarged sella turcica. There was a large adenoma that had poor

reticulin structure, and it stained strongly for GH (100%) and LH (10%–15%), whereas occasional cells were ACTH positive (Figure 4C). Prolactin staining was not found in the adenoma. The parenchyma surrounding the nodule exhibited diffuse somatotrope hyperplasia with enlarged trabeculae and stained for the different pituitary hormones, with the notable exception of prolactin.

Testis

The testes were of normal volume; macroscopically the tunica albuginea was thickened and there was a tunica vaginalis cyst on the right side. Microscopically, there was generalized atrophy of seminiferous tubes with an associated thickening of the basal membrane (Figure 5A). Multiple dark red/brown cysts were found close to the rete testis. These cysts were comprised of nodular Leydig cell hyperplasia; microcalcifications were also visible on light microscopy (Figure 5A). The hyperplastic cells stained positive for inhibin and the cytoplasm contained Reinke's crystalloid. The right testis contained a small area of normal parenchyma in which spermatogenesis was present (Figure 5, B and C).

Thyroid

The thyroid examination revealed homogenous multinodular goiter. Light microscopy displayed glandular hyperactivity with areas of colloidal pseudonodules.

Parathyroids

All four parathyroid glands were enlarged, which was shown to be due to nodular hyperplasia under microscopic examination (Figure 6A).

Endocrine pancreas

Hypertrophic and hyperplasic Langerhans islets were visualized in the tail of the pancreas (Figure 6B).

Adrenals

The adrenal glands exhibited bilateral cortical micronodular hyperplasia, as shown in Figure 6C.

Cardiovascular and respiratory systems

The heart was hypertrophic in appearance and hypertrophic cardiomegaly was confirmed histologically. No significant atherosclerosis was observed. Histological analysis of the right lung revealed recent infarction and edema caused by numerous microthrombi in the small vessels.

Gastrointestinal system

Three pseudopolyps with normal, nonhamartomatous (17), histological structure were present in the pylorus of the stomach. The liver was enlarged mainly due to congestion and cholestasis. Chronic pancreatitis with microlithiases was evident in the periphery of the head of the pancreas. Interestingly, islet cell hyperplasia was present. Immunohistochemical analysis did not detect increased population of endocrine cells in the lining of the stomach, duodenum and ileocecal region.

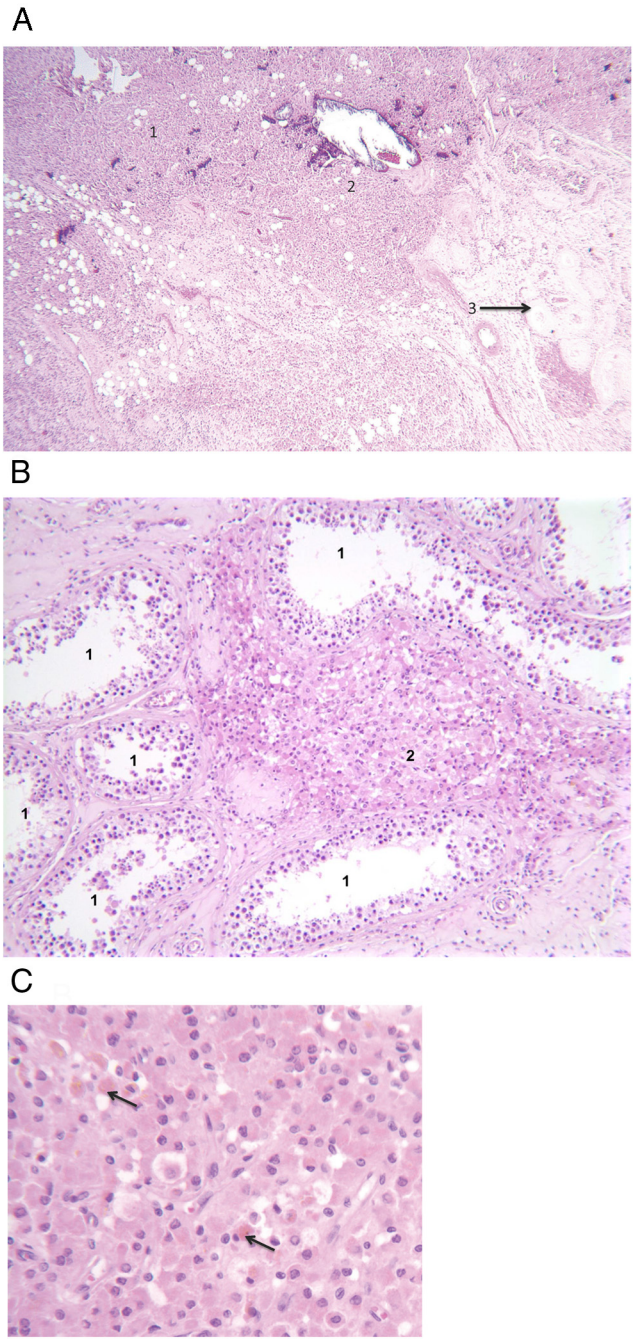

Figure 5. Panel A shows the testis, stained with hematoxylin and eosin (×25). Large nodule of Leydig cell hyperplasia (1) with multiple microliths (2) and residual atrophic seminiferous tubes (3). Panel B shows the testis stained with hematoxylin and eosin (×100). Seminiferous tubes with preserved complete spermatogenesis (1) are shown. Nodule of hyperplastic Leydig cells (2) is also shown. Panel C shows Leydig cell hyperplastic nodule at ×250 magnification with Reinke's crystalloid (arrows).

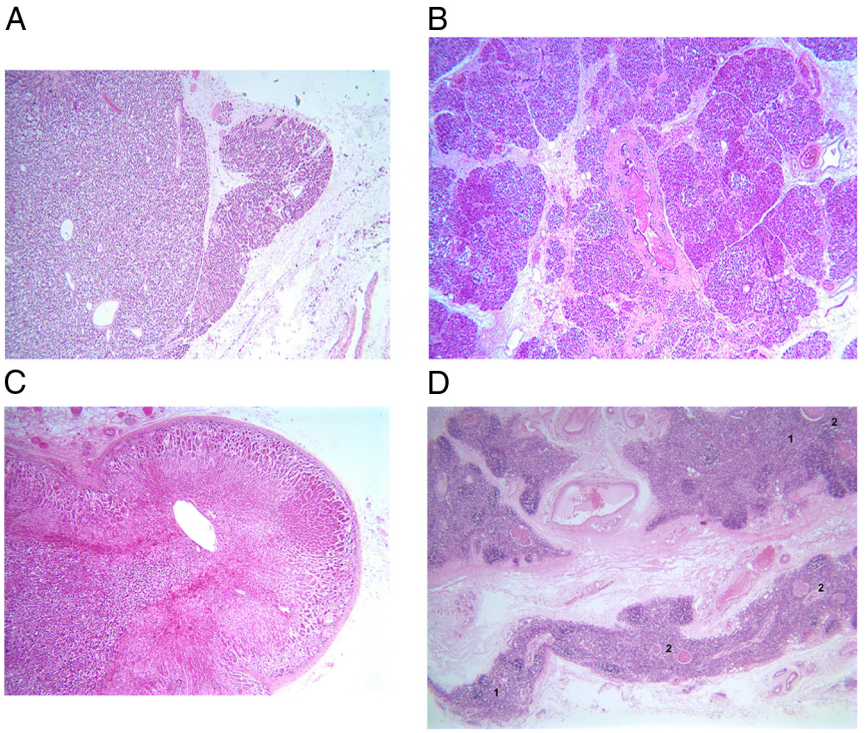

Figure 6. Panel A shows parathyroid gland stained with hematoxylin and eosin (×25) illustrating a region of nodular hyperplasia. Panel B shows pancreas stained with hematoxylin and eosin (×25) with extensive hyperplasia of the islets of Langerhans and associated calcifications. Panel C shows micronodular hyperplasia of the adrenal gland on hematoxylin and eosin stain (×25). Panel D shows thymus gland stained with hematoxylin and eosin (×25) and persistence of thymic tissue (1), Hassall's corpuscles (2) and epithelial hyperplasia.

Urinary system

Both kidneys were enlarged with signs of chronic pyelonephritis and medullary calcifications on light microscopy. No pathological findings were present in the prostate.

Immune system

The spleen was enlarged but microscopically normal. Remarkably for an adult patient, the thymus was intact and presented no signs of fat involution or atrophy (Figure 6D).

Mutation analysis

Paraffin-embedded and formalin-fixed samples from different organs were available for genetic study (Table 1). In pituitary adenoma and hyperplasia samples, DNA amplification was not possible due to DNA degradation. Heterozygous p.R201C mutation of the *GNAS1* gene was identified in several tumoral or pathologically abnormal samples, such as bone tumors and thyroid, parathyroid, thymus, and testis tissues. Pigmented skin was wild type, whereas apparently normal unpigmented skin bore the *GNAS1* mutation. Interestingly, tissues that are atypically/rarely involved in the MAS phenotype but that were pathologically affected in this case such as the pancreas, thymus, thyroid, and adrenals also had the *GNAS1* mutation in a mosaic distribution.

Discussion

MAS is a distinctive form of endocrine and nonendocrine neoplasia caused by a postzygotic mutation of the *GNAS1* gene, with affected cells being distributed in a mosaic pattern. This unique molecular pathophysiology leads to variability in the clinical expression and severity of disease features (3, 18, 19). Study of MAS differs from that of other endocrine neoplasia syndromes due to the lack of a robust animal model, meaning that the molecular pathology of the disease at an organ level is derived from painstaking study of clinical case collections. The current case underlines the importance of considering the myriad of possibly affected tissues. Additionally, this case highlights that in MAS patients, the disease impact might extend to atypical or rarely described sites such as the thymus, parathyroids, and pancreas. Indeed, in all three of these tissues, the use of newer PCR techniques (ddPCR), allowed us to demonstrate the presence of the *GNAS1* mutation in all three of these pathological tissues from this patient. In our patient the *GNAS1* mutation was identified in all but one affected organ and a mosaic distribution was confirmed. In the pituitary adenoma and hyperplasia, it was impossible to demonstrate the *GNAS1* mutation using either conventional or advanced PCR techniques because the DNA was too heavily degraded. Previously, conventional PCR techniques have failed to show *GNAS1* mutations in MAS patients despite diagnostic clinical features (14); we suggest that the use of techniques such as ddPCR could improve genetic diagnosis rates in suspected MAS patients.

Apart from the classical bone and skin involvement, our patient exhibited multiple endocrine abnormalities. The patient's most important endocrine abnormality was acrogigantism due to somatotrope hyperfunction and prolonged GH and IGF-1 excess (20). Acromegaly or gigantism occurs in a minority of cases of MAS, and recently Boyce et al (21) reported 26 of 129 (20.2%) of the National Institutes of Health (NIH) MAS cohort had GH excess, which confirms original estimates (22). Acromeg-

Table 1. Results from the Genetic Analysis of *GNAS1* in Endocrine and Nonendocrine Tissues

Tissue Source	Tissue Status	Finding at Position 201
Pigmented skin	Formalin fixed	Wild type
Normal skin	Formalin fixed	p.Arg201Cys heterozygous (G>A heterozygous)
Fat tissue	Formalin fixed	p.Arg201Cys heterozygous (G>A heterozygous)
Pancreas	Formalin fixed	p.Arg201Cys heterozygous (G>A heterozygous)
Pancreas	FFPE	Wild type
Bone	Formalin fixed	Wild type
Bone tumor 1	Formalin fixed	p.Arg201Cys heterozygous (G>A heterozygous)
Bone tumor 2	Formalin fixed	Wild type
Bone tumor 3	FFPE	p.Arg201Cys heterozygous (G>A heterozygous)
Bone tumor 4	Frozen	p.Arg201Cys heterozygous (G>A heterozygous)
Adrenal gland	Formalin fixed	p.Arg201Cys heterozygous (G>A heterozygous)
Adrenal gland	FFPE	wild type
Thyroid	Formalin fixed	p.Arg201Cys heterozygous (G>A heterozygous)
Thyroid	FFPE	p.Arg201Cys heterozygous (G>A heterozygous)
Heart	FFPE	Wild type
Parathyroid[a]	FFPE	p.Arg201Cys heterozygous (G>A heterozygous)
Thymus[a]	FFPE	p.Arg201Cys heterozygous (G>A heterozygous)
Testis[a]	FFPE	p.Arg201Cys heterozygous (G>A heterozygous)
Pituitary adenoma	FFPE	Unsuccessful
Pituitary hyperplasia	FFPE	Unsuccessful

Abbreviation: FFPE, formalin fixed, paraffin embedded.

[a] Using ddPCR (Bio-Rad Laboratories).

aly in MAS differs significantly from sporadic causes because pituitary abnormalities on MRI are often not present or are marginal despite advanced disease. In the current patient, multiple MRIs reported no abnormality of the sella and no adenoma. However, on autopsy a somatotrope adenoma surrounded by diffuse hyperplasia was discovered. This underlines the recent conclusions of Vortmeyer et al (9) that pituitary disease in MAS is a diffuse and varied pathology. The disconnect between imaging and direct visualization may be due to deformation by FD interfering with sellar imaging. The pituitary in the current case exhibited the typical somatotrope hyperplasia that constitutes the primary abnormality in acromegaly in MAS. Some patients may have somatomammotrope hyperplasia; in the current case, no prolactin staining was seen, although this may have been due to chronic cabergoline treatment. The craniofacial FD in this case continued to advance during the patient's third and fourth decade, with deformity leading to monocular blindness and hearing impairment.

The issue of craniofacial FD and GH excess in MAS has received consistent attention (18, 22–26). The dramatic craniofacial FD that developed in this adult patient (Figures 2–4) is in keeping with the harmful role of GH excess on cranial bone pathology in MAS patients. Recent data indicate that MAS patients with GH excess that have early intervention (<18 y of age) to control GH/IGF-1 have decreased risk of optic neuropathy (21). Among 22 subjects with significant somatotrope hyperfunction in the NIH cohort, 15 had intervention before the age of 18 years (early) and the other seven after the age of 18 years (late). Notably the subjects with late intervention for GH control had a significantly larger head circumference than the early intervention or control MAS groups. This indicates that earlier control of somatotrope axis hyperfunction can slow the underlying FD growth and limit craniofacial distortion. This finding is echoed in the experience of the current patient, who had late control of somatotrope axis hyperfunction. In his case, control of GH excess was not medically achievable in childhood/adolescence because somatostatin analogs were not available. Current guidelines recommend that GH/IGF-1 control should be prioritized to potentially prevent worsening of craniofacial FD. This is also to prevent the worsening of other conditions like cardiac muscle dysfunction/cardiomyopathy, to which both acromegaly and *GNAS1* mutations can contribute. Some patients respond well to long-acting somatostatin analogs (27), but somatostatin analog resistance has been reported, and in those cases GH receptor antagonist treatment (27, 28) or combined medical therapy (29) can be successful.

Hyperprolactinemia has been associated with GH hypersecretion in most MAS patients (22) as well as in sporadic somatotrope tumors bearing the *gsp* oncogene (22, 30). The absence of prolactin on immunohistochemistry in our case may be due to cabergoline treatment. Dopamine agonists can help in controlling hyperprolactinemia, but do not appear to provide significant benefit in GH/IGF-1 control. Radiotherapy in MAS is limited by concerns over malignant transformation of fibrodysplastic bone when radiotherapy is used (31). Surgery can be complicated because of not only the significant bone overgrowth and anatomical distortion but also because acromegaly in MAS is primarily due to somatotrope or somatomammotrope hyperplasia. Hence, adenoma resection may not be curative or an adenoma may not be present. In intractable cases, hypophysectomy has been suggested as a curative option when all other avenues have been exhausted (9).

Peripheral precocious puberty is one of the hallmarks of MAS and was the main endocrine abnormality that led to the recognition of the disease in the 1930s (1, 2). It has a high prevalence in females with MAS, possibly because both granulosa and theca cell are steroidogenically competent and subject to activation. In the testes, the Leydig cells must carry the activating mutation to trigger precocious androgen synthesis (32, 33). Sertoli cell-only mutations may be responsible for testicular enlargement without signs of peripheral hyperandrogenism (34, 35). Leydig cell hyperplasia and focal spermatogenesis have been described in MAS for many years (5), and testicular microlithiasis was proposed as an additional pathological marker in males (36). The testicular phenotype in MAS has recently been elucidated in the clinical setting by Boyce et al (10) in 54 males from the NIH cohort. They confirmed that testicular ultrasound abnormalities were present in 81% of cases, with hyperechoic lesions and testicular heterogeneity in 45%–47% of cases. Bilateral disease occurred in 75%, and 44% had macroorchidism, again usually bilaterally. Microlithiasis and/or focal calcification were also characterized as occurring in 30% and 10% of cases, respectively. On pathological examination of surgical tissue (orchiectomy, biopsy, or autopsy material), Leydig cell hyperplasia was found in seven of eight cases (87.5%), similar to the extensive disease in the current case. The picture of sclerosis, localized Leydig cells hyperplasia, and microcalcifications in our case are therefore typical of gonadal effects in an adult male MAS patient (Reinke crystalloid was not previously noted to our knowledge). Although dramatic gonadal changes occur in most males with MAS, the longitudinal follow-up is encouraging, with testicular malignancy being rare in the NIH cohort, and in the rare occasion in which testicular cancer did occur, the long-term response to therapy was good.

In the current case, the thymus showed no signs of the involution that would normally be expected in an adult, and the *GNAS1* mutation was shown in the thymic tissue. GH itself is recognized to have a regulatory role in thymic tissue growth, and thymic hyperplasia has been reported in acromegaly and growth hormone treatment (37–39). Whether persistence of the thymus in this case was due to a primary effect of MAS or secondary to GH hypersecretion is uncertain and requires study in larger cohorts. A similarly intriguing finding was that of primary hyperparathyroidism associated with parathyroid hyperplasia, and again more advanced PCR techniques showed the *GNAS1* mutation to be present in the hyperplastic tissue. Primary hyperparathyroidism has been reported only once in the NIH cohort, so the addition of this genetically confirmed case due to multiglandular parathyroid hyperplasia suggests that it may form a rare association in MAS (3). A *GNAS1* mutation was also detected in the thyroid and adrenal glands as well as the pancreas, but, despite being associated with hyperplasia or histological abnormalities (islet cell hyperplasia), they were not associated with hormonal hypersecretion. The bilateral adrenal hyperplasia that was found at autopsy in the patient was unaccompanied by clinical or other evidence of overt Cushing's syndrome during his lifetime. However, as reported by Brown et al (40), Cushing's syndrome in MAS can arise and later resolve spontaneously, leaving adrenal abnormalities and residual adrenal dysfunction. No specific tests were performed to identify such residual biochemical abnormalities during the patient's lifetime.

Variable disease burden in MAS may be explained by mosaicism in the affected organs, low expression of the mutant allele in some tissues (41), interfering molecular mechanism such as the increase in phosphodiesterase activity (5, 42, 43), or possibly due to variable cell specific consequences of increased cAMP production. According to interactions between MAPK and cAMP pathways, the cAMP increase could induce cell proliferation or differentiation, depending on particular cell phenotype (44). Despite the widespread endocrine and nonendocrine pathology in this case, no tumors of the exocrine pancreas or hepatobiliary system were seen, confirming that such tumors occur in a minority of MAS cases (32%) (45).

In conclusion, the present case study, which incorporated a comprehensive clinical, pathologic, and genetic analysis of an adult male patient with MAS, underlines the variable tissue-specific sensitivity to *GNAS1* mutation in humans and illustrates the current clinical understanding of the consequences of disease activity and treatment of this remarkably challenging disease.

Acknowledgments

Address all correspondence and requests for reprints to: Professor Albert Beckers, MD, PhD, Department of Endocrinology, Centre Hospitalier Universitaire de Liège, University of Liège, Domaine Universitaire du Sart-Tilman, 4000 Liège, Belgium. E-mail: albert.beckers@chu.ulg.ac.be.

This work was supported in part by grants from the Fonds d'Investissement pour la Recherche Scientifique 2010–2012 of the Centre Hospitalier Universitaire de Liège, University of Liège, Belgium; Pfizer S.A., Belgium; and the Oncogenetic Network of the French Ministry of Health, Centre National de la Recherche Scientifique.

Disclosure Summary: The authors have nothing to declare.

References

1. **McCune DJ.** Osteita fibrosa cystica : the case of nine-year-old girl who also exhibits precocious puberty, multiple pigmentation of the skin and hyperthyroidism. *Am J Dis Child*. 1936;52:743–744.

2. **Albright F, Butler AM, Hampton AO, Smith P.** Syndrome characterized by osteitis fibrosa disseminata, areas of pigmentation and endocrine dysfunction, with precocious puberty in females. *N Engl J Med*. 1937;216(17):727–746.
3. **Collins MT, Singer FR, Eugster E.** McCune-Albright syndrome and the extraskeletal manifestations of fibrous dysplasia. *Orphan J Rare Dis*. 2012;7(suppl 1):S4.
4. **Shenker A, Weinstein LS, Moran A, et al.** Severe endocrine and nonendocrine manifestations of the McCune-Albright syndrome associated with activating mutations of stimulatory G protein GS. *J Pediatr*. 1993;123(4):509–518.
5. **Weinstein LS, Shenker A, Gejman PV, Merino MJ, Friedman E, Spiegel AM.** Activating mutations of the stimulatory G protein in the McCune-Albright syndrome. *N Engl J Med*. 1991;325(24):1688–1695.
6. **Schwindinger WF, Francomano CA, Levine MA.** Identification of a mutation in the gene encoding the alpha subunit of the stimulatory G protein of adenylyl cyclase in McCune-Albright syndrome. *Proc Natl Acad Sci USA*. 1992;89(11):5152–5156.
7. **Ringel MD, Schwindinger WF, Levine MA.** Clinical implications of genetic defects in G proteins. The molecular basis of McCune-Albright syndrome and Albright hereditary osteodystrophy. *Medicine*. 1996;75(4):171–184.
8. **Lumbroso S, Paris F, Sultan C, European Collaborative S.** Activating Gsα mutations: analysis of 113 patients with signs of McCune-Albright syndrome—a European Collaborative Study. *J Clin Endocrinol Metab*. 2004;89(5):2107–2113.
9. **Vortmeyer AO, Glasker S, Mehta GU, et al.** Somatic GNAS mutation causes widespread and diffuse pituitary disease in acromegalic patients with McCune-Albright syndrome. *J Clin Endocrinol Metab*. 2012;97(7):2404–2413.
10. **Boyce AM, Chong WH, Shawker TH, et al.** Characterization and management of testicular pathology in McCune-Albright syndrome. *J Clin Endocrinol Metab*. 2012;97(9):E1782–E1790.
11. **Shedlock AM, Haygood MG, Pietsch TW, Bentzen P.** Enhanced DNA extraction and PCR amplification of mitochondrial genes from formalin-fixed museum specimens. *Biotechniques*. 1997;22(3):394–396, 398, 400.
12. **Satoh Y, Takasaka N, Hoshikawa Y, et al.** Pretreatment with restriction enzyme or bovine serum albumin for effective PCR amplification of Epstein-Barr virus DNA in DNA extracted from paraffin-embedded gastric carcinoma tissue. *J Clin Microbiol*. 1998;36(11):3423–3425.
13. **Candeliere GA, Roughley PJ, Glorieux FH.** Polymerase chain reaction-based technique for the selective enrichment and analysis of mosaic arg201 mutations in Gαs from patients with fibrous dysplasia of bone. *Bone*. 1997;21(2):201–206.
14. **Kalfa N, Philibert P, Audran F, et al.** Searching for somatic mutations in McCune-Albright syndrome: a comparative study of the peptidic nucleic acid versus the nested PCR method based on 148 DNA samples. *Eur J Endocrinol*. 2006;155(6):839–843.
15. **Vogelstein B, Kinzler KW.** Digital PCR. *Proc Natl Acad Sci USA*. 1999;96(16):9236–9241.
16. **Hussein SM, Batada NN, Vuoristo S, et al.** Copy number variation and selection during reprogramming to pluripotency. *Nature*. 2011;471(7336):58–62.
17. **Zacharin M, Bajpai A, Chow CW, et al.** Gastrointestinal polyps in McCune Albright syndrome. *J Med Genet*. 2011;48(7):458–461.
18. **Dumitrescu CE, Collins MT.** McCune-Albright syndrome. *Orphan J Rare Dis*. 2008;3:12.
19. **Salpea P, Stratakis CA.** Carney complex and McCune Albright syndrome: an overview of clinical manifestations and human molecular genetics. *Mol Cell Endocrinol*. 2014;386(1–2):85–91.
20. **Horvath A, Stratakis CA.** Clinical and molecular genetics of acromegaly: MEN1, Carney complex, McCune-Albright syndrome, familial acromegaly and genetic defects in sporadic tumors. *Rev Endocr Metab Disord*. 2008;9(1):1–11.
21. **Boyce AM, Glover M, Kelly MH, et al.** Optic neuropathy in McCune-Albright syndrome: effects of early diagnosis and treatment of growth hormone excess. *J Clin Endocrinol Metab*. 2013;98(1):E126–E134.
22. **Akintoye SO, Chebli C, Booher S, et al.** Characterization of gsp-mediated growth hormone excess in the context of McCune-Albright syndrome. *J Clin Endocrinol Metab*. 2002;87(11):5104–5112.
23. **Akintoye SO, Boyce AM, Collins MT.** Dental perspectives in fibrous dysplasia and McCune-Albright syndrome. *Oral Surg Oral Med Oral Pathol Oral Radiol*. 2013;116(3):e149–e155.
24. **Akintoye SO, Otis LL, Atkinson JC, et al.** Analyses of variable panoramic radiographic characteristics of maxillo-mandibular fibrous dysplasia in McCune-Albright syndrome. *Oral Dis*. 2004;10(1):36–43.
25. **DeKlotz TR, Kim HJ, Kelly M, Collins MT.** Sinonasal disease in polyostotic fibrous dysplasia and McCune-Albright Syndrome. *Laryngoscope*. 2013;123(4):823–828.
26. **Leet AI, Collins MT.** Current approach to fibrous dysplasia of bone and McCune-Albright syndrome. *J Child Orthopaed*. 2007;1(1):3–17.
27. **Chanson P, Dib A, Visot A, Derome PJ.** McCune-Albright syndrome and acromegaly: clinical studies and responses to treatment in five cases. *Eur J Endocrinol*. 1994;131(3):229–234.
28. **Akintoye SO, Kelly MH, Brillante B, et al.** Pegvisomant for the treatment of gsp-mediated growth hormone excess in patients with McCune-Albright syndrome. *J Clin Endocrinol Metab*. 2006;91(8):2960–2966.
29. **Galland F, Kamenicky P, Affres H, et al.** McCune-Albright syndrome and acromegaly: effects of hypothalamopituitary radiotherapy and/or pegvisomant in somatostatin analog-resistant patients. *J Clin Endocrinol Metab*. 2006;91(12):4957–4961.
30. **Barlier A, Gunz G, Zamora AJ, et al.** Pronostic and therapeutic consequences of Gs alpha mutations in somatotroph adenomas. *J Clin Endocrinol Metab*. 1998;83(5):1604–1610.
31. **Hansen MR, Moffat JC.** Osteosarcoma of the skull base after radiation therapy in a patient with McCune-Albright syndrome: case report. *Skull Base*. 2003;13(2):79–83.
32. **Wasniewska M, Matarazzo P, Weber G, et al.** Clinical presentation of McCune-Albright syndrome in males. *J Pediatr Endocrinol Metab*. 2006;19(suppl 2):619–622.
33. **Rey RA, Venara M, Coutant R, et al.** Unexpected mosaicism of R201H-GNAS1 mutant-bearing cells in the testes underlie macroorchidism without sexual precocity in McCune-Albright syndrome. *Hum Mol Genet*. 2006;15(24):3538–3543.
34. **Coutant R, Lumbroso S, Rey R, et al.** Macroorchidism due to autonomous hyperfunction of Sertoli cells and G(s)α gene mutation: an unusual expression of McCune-Albright syndrome in a prepubertal boy. *J Clin Endocrinol Metab*. 2001;86(4):1778–1781.
35. **Arrigo T, Pirazzoli P, De Sanctis L, et al.** McCune-Albright syndrome in a boy may present with a monolateral macroorchidism as an early and isolated clinical manifestation. *Horm Res*. 2006;65(3):114–119.
36. **Wasniewska M, De Luca F, Bertelloni S, et al.** Testicular microlithiasis: an unreported feature of McCune-Albright syndrome in males. *J Pediatr*. 2004;145(5):670–672.
37. **Timsit J, Savino W, Safieh B, et al.** Growth hormone and insulin-like growth factor-I stimulate hormonal function and proliferation of thymic epithelial cells. *J Clin Endocrinol Metab*. 1992;75(1):183–188.
38. **Napolitano LA, Lo JC, Gotway MB, et al.** Increased thymic mass and circulating naive CD4 T cells in HIV-1-infected adults treated with growth hormone. *AIDS*. 2002;16(8):1103–1111.
39. **Polgreen L, Steiner M, Dietz CA, Manivel JC, Petryk A.** Thymic hyperplasia in a child treated with growth hormone. *Growth Horm IGF Res*. 2007;17(1):41–46.

40. **Brown RJ, Kelly MH, Collins MT.** Cushing syndrome in the McCune-Albright syndrome. *J Clin Endocrinol Metab*. 2010;95(4):1508–1515.
41. **Ballare E, Mantovani S, Lania A, Di Blasio AM, Vallar L, Spada A.** Activating mutations of the Gs α gene are associated with low levels of Gs α protein in growth hormone-secreting tumors. *J Clin Endocrinol Metab*. 1998;83(12):4386–4390.
42. **Lania A, Persani L, Ballare E, Mantovani S, Losa M, Spada A.** Constitutively active Gs α is associated with an increased phosphodiesterase activity in human growth hormone-secreting adenomas. *J Clin Endocrinol Metab*. 1998;83(5):1624–1628.
43. **Lania AG, Mantovani G, Spada A.** Mechanisms of disease: Mutations of G proteins and G-protein-coupled receptors in endocrine diseases. *Nat Clin Pract Endocrinol Metab*. 2006;2(12):681–693.
44. **Stork PJ, Schmitt JM.** Cross talk between cAMP and MAP kinase signaling in the regulation of cell proliferation. *Trends Cell Biol*. 2002;12(6):258–266.
45. **Gaujoux S, Salenave S, Ronot M, et al.** Hepatobiliary and pancreatic neoplasms in patients with McCune-Albright syndrome. *J Clin Endocrinol Metab*. 2014;99(1):E97–E101.